NSNI Mitigation in Bi-Directional Raman Amplified Unrepeatered System Using Split-DBP

Qiang Zheng, Liyan Huang, Wei Li, Qiguang Feng, Chengpeng Fu, and Jiekui Yu

***Abstract*—The nonlinear signal–noise interaction (NSNI) is analyzed in the bi-directional Raman amplified unrepeatered system with digital back-propagation (DBP) algorithm. When the DBP is applied at the receiver side, because in the DBP process the spontaneous Raman scattering is not dealt with, extra NSNI occurs, and because of the high power in the system, the extra NSNI is severe. By adopting split-DBP, the interaction of noise and signal in the high-power region could be avoided. Thus, the extra NSNI was mitigated and the performance was improved. The performance of split-DBP algorithm in such a system was investigated through simulations and experiments, using a single-channel 300-km bi-directional Raman amplified unrepeatered system. The simulations were carried out with 16 QAM modulation and the modulation rates were 32 GBd and 10 GBd. The results showed that the split-DBP can deliver 0.8-dB Q^2-factor improvement for the case of 32 GBd and 1.3 dB for the case of 10 GBd, compared to the traditional DBP. The impact of the nonlinear transform function of modulator and power profile mismatch on the performance of split-DBP is discussed through the simulation, which is critical to the practical implementation of split-DBP. An experimental demonstration of the split-DBP with 10 GBd 16 QAM modulation was carried out. The experimental results presented a 1.2-dB Q^2-factor improvement of the signal due to split-DBP.**

***Index Terms*—Digital back-propagation, nonlinear signal-to-noise interaction, nonlinearity mitigation, optical fiber communications, Raman amplification.**

I. Introduction

BY VIRTUE of rapid development of DSP chip, in optical fiber communication systems, modern DSP-based coherent receivers can fully compensate for the linear channel impairments, such as chromatic dispersion (CD) and polarization mode dispersion (PMD) [1], [2]. Consequently, nonlinear impairments, which include mainly Kerr effects, such as self-phase modulation (SPM), cross-phase modulation (XPM) and four-wave mixing (FWM), limit the transmission performance [3]. Digital back-propagation (DBP) algorithm is now commonly acknowledged as one of the most suitable candidates for joint linear and nonlinear impairment compensation [4]–[6]. Consequently, several modified schemes of DBP, such as low-complexity DBP [7], correlated DBP [8], and adaptive DBP [9], have been proposed either for improving performance or for reducing computational complexity.

However, for the traditional DBP algorithms mentioned above, noises in the system, such as Amplified Spontaneous Emission (ASE) and transceiver noise, are not taken into account. In practical optical fiber communication system, such noises in the fiber would interact with the signal through the Kerr effect, which is called nonlinear signal-noise interaction (NSNI). As the noises are not considered in the traditional DBP algorithm, the NSNI induced by the noises cannot be dealt with. Moreover, once the DBP algorithm was applied to the system, the noises would continue interacting with the signal during the DBP process, thus causing extra NSNI. There has been a study of the impact of the transceiver noise on the performance of DBP, which indicates that the transceiver noise would induce extra NSNI in the receiver-side DBP, thus limiting the performance of DBP [10].

Recently, an algorithm, called stochastic DBP, was proposed to compensate for the NSNI caused by the EDFAs in the link, but complex probability method was required [11]. Considering the computational complexity of stochastic DBP, another easier approach called split-DBP was proposed and studied, which involves moving a part of DBP from the receiver side to the transmitter side. By this means, part of the NSNI can be avoided and the performance is improved [12]–[14]. In [13], D. Lavery *et al.* demonstrated that split nonlinear compensation scheme is better than both post and pre- compensation schemes in EDFA amplified systems through simulation. However, the study was confined to investigating only EDFA amplified systems, but not Raman amplified system.

Distributed Raman amplification is regarded as a mature and promising amplification scheme for next-generation fiber optical communication systems [15], [16]. Especially for the ultra-long span unrepeatered system, the distributed Raman amplification is the critical technology. For the ultra-long span unrepeatered system, because the loss of the link is large, the incident power must be high enough to ensure the receiver works properly. Thus the fiber nonlinearity is an issue impacting the signal. Moreover, in such a system, to make the transmission as long as possible, the optical signal-to-noise ratio (OSNR) at the receiver side is usually just near the limiting value, which means

Manuscript received November 8, 2017; revised March 3, 2018 and May 26, 2018; accepted June 6, 2018. Date of publication June 13, 2018; date of current version June 29, 2018. This work was supported in part by the China 863 Project (2015AA017002) and in part by the Research Foundation of Wuhan Science and Technology Bureau (2015010303010141). *(Corresponding author: Wei Li.)*

Q. Zhen, W. Li, and Q. Feng are with the Wuhan National Laboratory for Optoelectronics, Huazhong University of Science and Technology, Wuhan 430074, China (e-mail: zheng_qiang@foxmail.com; weilee@hust.edu.cn; feng_qiguang@yeah.net).

L. Huang, C. Fu, and J. Yu are with Accelink Technologies Co., Ltd., Wuhan 430205, China (e-mail: liyan.huang@accelink.com; chengpeng.fu@accelink.com; jiekui.yu@accelink.com).

Color versions of one or more of the figures in this paper are available online at http://ieeexplore.ieee.org.

Digital Object Identifier 10.1109/JLT.2018.2846691

the noise in the system is severe. As a result, the NSNI in Raman amplified systems is also a critical issue. The DBP algorithm has been applied in Raman amplified unrepeatered system for nonlinearity compensation [17], [18], but the NSNI is ignored.

This study analyzed the NSNI, induced by the transceiver noise and the spontaneous Raman scattering in bi-directional Raman amplified unrepeatered systems with DBP. The origin of the extra NSNI in the system was studied. Theoretical analysis indicates that the extra NSNI can be effectively mitigated by moving the high power region of DBP form the receiver side to the transmitter side, namely split-DBP. Then the performance of the split-DBP was investigated through simulations, using a bi-directional Raman amplified system with 32 GBd 16 QAM modulation. And two critical issues of practical implementation of split-DBP in bi-directional Raman amplified system were discussed through simulation. Finally, an experimental demonstration of split-DBP in bi-directional Raman amplified unrepeatered system was carried out.

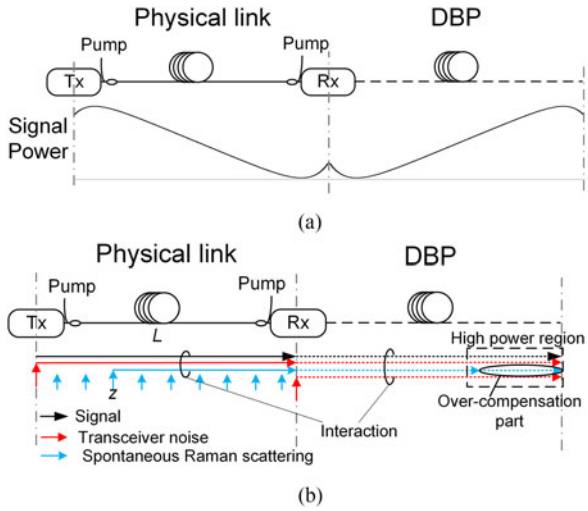

Fig. 1. (a) Bi-directional Raman system with DBP, (b) NSNI in bi-directional Raman system with DBP.

II. Principles

A. NSNI in Bi-Directional Raman Amplified System With DBP

In the optical communication system, noises not only impact the OSNR at the receiver side, but also interact with the signal along the fiber due to fiber nonlinearity, i.e., NSNI. NSNI was initially considered in long-haul transmission system with EDFAs. The noise from EDFAs accumulates along the fiber and is converted to phase noise under the Kerr effects in fiber [19]. In the system with DBP, the noises and the signal, propagating through a virtual fiber, will also bring NSNI to the signal, in the same way as they bring NSNI in the practical fiber. In such a situation, the NSNI will have two parts, one from practical fiber and the other from DBP (or virtual fiber).

In the EDFA amplified system, the noises include mainly the ASE from EDFAs and the noise from the transceiver. Their impact on the signal, both linear and nonlinear, can be accurately estimated. But in the bi-directional Raman amplified system, the noises include the transceiver noise, spontaneous Raman scattering, relative intensity noise (RIN) transfer from the pump to the signal and double Rayleigh scattering. These noises are based on different optical effects and amplified by the Raman pump. It is complex to include all these noises in the analysis. For simplicity, in the analysis that follows, only transceiver noise, and spontaneous Raman scattering are taken into account. The results can be extended to the condition of double Rayleigh backscattering, because its statistical characteristic is nearly a complex Gaussian distribution and can be treated as ASE [19].

Figure 1(a) illustrates a typical bi-directional Raman amplified system, with receiver-side DBP, and (b) illustrates the NSNI in such a system. In Fig. 1(b), the solid lines correspond to the practical fiber, and the dotted lines to the virtual fiber in DBP; the signal and noise are shown below the block diagram of the system by arrows of different colors; the black arrows represent the signal, the red arrows the transceiver noise, which includes transmitter noise and receiver noise, and the blue arrows the spontaneous Raman scattering generated in fiber. When the signals and noises propagate through both the practical and virtual fibers, they will mutually interact under fiber nonlinearity. It should be noted that the interaction in the practical fiber is opposite to that in the virtual fiber.

As regards transmitter noise, it travels along the fiber, as shown in Fig. 1(b). Its interactions with signal in practical and virtual fibers are opposite and will counteract with each other; in other words, the DBP compensates fully for the NSNI caused by the transmitter noise. Similarly, for the noise generated in the fiber at point z, as the blue arrow in Fig. 1(b) shown, will propagate along the fiber with a length of L-z and interacts with the signal, where L is the length of the whole fiber. After virtual transmission in DBP with a same length of L-z, the NSNI caused by the noise at point z is completely compensated. But, the noise continues to propagate and interact with the signal in the residual virtual fiber of length z, causing an obvious over-compensation part. Because of the amplification of the forward Raman amplifier, the signal power in the front part of the fiber is very high, and in the DBP process the high power region is at the end, which is shown as dashed line box in Fig. 1(b). Unfortunately, most of the over-compensation parts are in the high power region. Thus, the over-compensation parts will produce intense extra NSNI and impair the performance of signal. For the receiver noise, it propagates and interacts with the signal only in the virtual fiber and the DBP is an entire over-compensation procedure.

To conclude, for the bi-directional Raman amplified system, the DBP algorithm can compensate fully for the NSNI caused by the transmitter noise. But, for the noises from the fiber and receiver, the DBP would generate extra NSNI. And, the extra NSNI originates at such a point for which there is no method to remove noise at the position symmetrical to it in the practical link.

B. Split-DBP for NSNI Mitigation

As described above, in bi-directional Raman amplified systems, DBP produces extra NSNI because of the

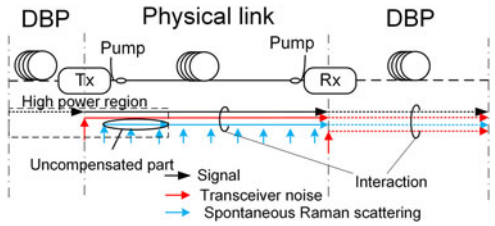

Fig. 2. Split-DBP for bi-directional Raman amplified system.

over-compensation, and intense extra NSNI occurs in the high power region. It is obvious that the intensity of extra NSNI is relative to the noise near the receiver side and the peak power of signal. In the bi-directional Raman amplified unrepeatered system, the peak power of signal should be high enough to maintain the OSNR requirement of the receiver, where the extra NSNI cannot be ignored.

To deal with the extra NSNI, the DBP of high power region can be moved from the receiver side to the transmitter side, as shown in Fig. 2. By this means, the extra NSNI caused by the over-compensation of the receiver-side DBP in the high power region is avoided. Even the remaining receiver-side DBP still causes extra NSNI in the same manner, because the power in the remaining receiver-side DBP is low, the extra NSNI is small.

On the other hand, the transmitter-side DBP will cause residual NSNI, because the NSNI caused by the noise generated near the transmitter is not compensated, as shown in Fig. 2. As the noise near the receiver is stronger than the one near the transmitter, the residual NSNI is weaker than the extra NSNI caused by receiver-side DBP. Consequently, the whole NSNI of the system decreases. It is obvious that there is an optimal split ratio of DBP for the best performance, which is discussed in Section IV-B.

III. Simulations Setup

In order to assess the performance of split-DBP in bi-directional Raman amplified system, numerical simulations were carried out, with the simulated system in Fig. 3. In the transmitter, a laser with a linewidth of 100 kHz and an ideal IQ modulator were assumed to generate the signal. A single-channel 32 Gbaud 16 QAM signal was generated with a pseudo-random binary sequence of length $2^{15}-1$. The signal was sampled at 8 samples/symbol and filtered by a Gaussian low-pass filter for pulse shaping. Two EDFAs, each with a noise figure of 4 dB, were deployed as booster amplifier and pre-amplifier before the transmission link and before the coherent receiver. The transmission link was a 300-km long standard single mode fiber, with attenuation coefficients of $0.2\,\mathrm{dB}\cdot\mathrm{km}^{-1}$ for signal and $0.26\,\mathrm{dB}\cdot\mathrm{km}^{-1}$ for pump, dispersion coefficient $17\,\mathrm{ps}\cdot\mathrm{nm}^{-1}\cdot\mathrm{km}^{-1}$ and nonlinear coefficient $1.1\,\mathrm{W}^{-1}\cdot\mathrm{km}^{-1}$. The signal propagation in the fiber was simulated by solving the modified nonlinear Schrödinger equation using the split step Fourier method (SSFM):

$$\frac{\partial A(z,T)}{\partial z} = \left(-\frac{\alpha_s}{2}+G(z)\right)A(z,T) - \frac{i\beta_2}{2}\frac{\partial^2 A(z,T)}{\partial T^2} + i\gamma|A(z,T)|^2 A(z,T) \quad (1)$$

where $A(z,T)$ is the electric field of the signal, α_s is the fiber attenuation coefficient of the signal, $G(z)$ is the distributed Raman gain, β_2 is the group velocity dispersion parameter, and γ is the fiber nonlinear parameter. The wavelengths of signal and pump are 1550 nm and 1455 nm. The distributed Raman gain was calculated by solving the power coupled equations of distributed Raman amplifier [20], [equation 8.1.2–8.1.3]:

$$\frac{dP_s}{dz} = -\alpha_s P_s + g_R(P_p^+ + P_p^-)P_s$$
$$\pm\frac{dP_p^\pm}{dz} = -\alpha_p P_p^\pm - \frac{\omega_p}{\omega_s} g_R P_p^\pm P_s \quad (2)$$

where P_s is the signal power, P_p is the pump power, "+" and "−" denote the forward Raman and backward Raman pump, respectively, α_p is the attenuation coefficient of the pump, $\omega_{p,s}$ denotes the angular frequency of the pump/signal, and g_R is the Raman gain coefficient, which was set 0.79 km/W. In the simulation, the forward Raman gain was 12.4 dB, and the backward Raman gain was 16.6 dB, respectively. After solving equations (2), we can get the signal power, and the distributed Raman gain can be calculated by:

$$G(z) = \frac{1}{2P_s}\cdot\frac{dP_s}{dz} + \frac{\alpha_s}{2} \quad (3)$$

The RIN transfer from the Raman pump to the signal was simulated by a time variation of the distributed Raman gain. The time variation was produced by multiplying the RIN of the pump laser and the RIN transfer function (TF) from the pump to the signal [21]. The RIN of the pump laser was set −120 dBc/Hz. The step size of the SSFM was 0.01 km and in each step spontaneous Raman scattering was added to the signal. After transmission an optical band-pass filter (OBPF) was deployed with a bandwidth of 100 GHz. In the coherent receiver another laser with the same parameters as the transmitter laser was used as local oscillator. The photodetectors in the receiver were modeled with ideal response properties, and thermal noise and shot noise were considered. Then the received signal was down-sampled to 2 samples/symbol for subsequent DSP.

In the receiver DSP carrier recovery was applied to compensate for the phase shift of the laser. Two nonlinear compensation methods were applied in the simulation: receiver-side DBP and split-DBP, and both of them were compared with the electronic dispersion compensation (EDC) condition. To fairly compare the performance of receiver-side DBP and split-DBP, in the split-DBP scheme, the signal was processed by the transmitter-side DBP at 2 samples/symbol, and then the processed signal was up-sampled to 8 samples/symbol for fiber transmission. Bit error rate (BER) of the signal was calculated after the DSP.

IV. Results and Discussion

A. The Performance of Split-DBP

In the split-DBP scheme, the compensation length of transmitter-side DBP was 70 km for each incident power, corresponding to the optimum pre-compensation length. And, the step number of receiver-side DBP was 20, while the step number

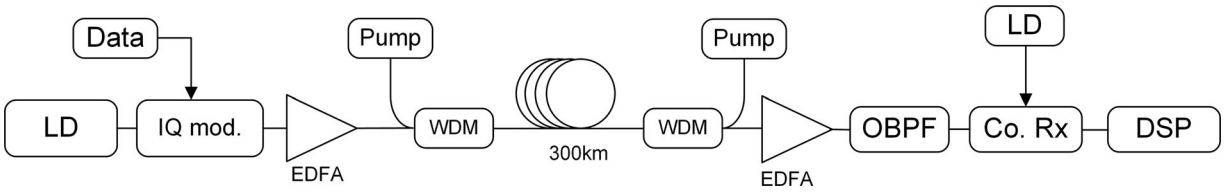

Fig. 3. Simulation setup: LD- laser diode; IQ mod.- IQ modulator; OBPF- optical band-pass filter; Co. Rx- coherent receiver.

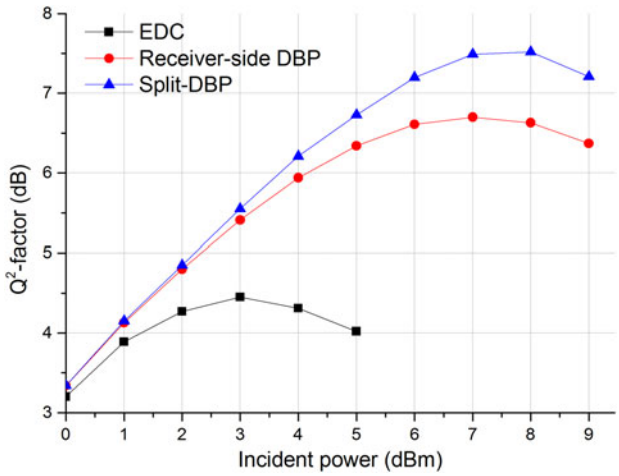

Fig. 4. Q^2-factor vs. incident power in the simulations, with different compensation schemes.

of split-DBP was 10 each, for the transmitter-side and receiver-side DBPs. The results are shown in Fig. 4.

From this figure it can be seen that, with the complete receiver-side DBP, the Q^2-factor of the signal improved by 2.1 dB compared to that of the EDC condition. This is because, the nonlinearity of signal itself, mainly the SPM, was compensated by DBP. With the split-DBP scheme, the Q^2-factor of the signal improved by 0.8 dB, compared to that of the complete receiver-side DBP, and by 2.9 dB, compared to that of the dispersion compensation case. And, the optimal incident power of split-DBP increased by 1 dBm, compared to that of the complete receiver-side DBP.

Comparison of the curves of split-DBP and complete receiver-side DBP shows that, when the incident power was lower than 2 dBm, their performances were nearly the same. This suggests that, in the low power region, the extra NSNI can be ignored. When the incident power is higher than 2 dBm, extra NSNI does emerge, but not very severe. The Q^2-factor of the signal continues to rise in the complete receiver-side DBP scheme, and the performance of the split-DBP becomes better than that of the complete receiver-side DBP. When the incident power is over 7 dBm, the extra NSNI will be very severe and the Q^2-factor of complete receiver-side DBP starts decreasing. For the split-DBP scheme, with the extra NSNI mitigated, the Q^2-factor continues to rise until the incident power is 8 dBm. When the incident power exceeds 8 dBm, the performance of split-DBP starts degrading, because split-DBP scheme cannot completely remove the NSNI, and other high order nonlinear impairments appear and can not be compensated.

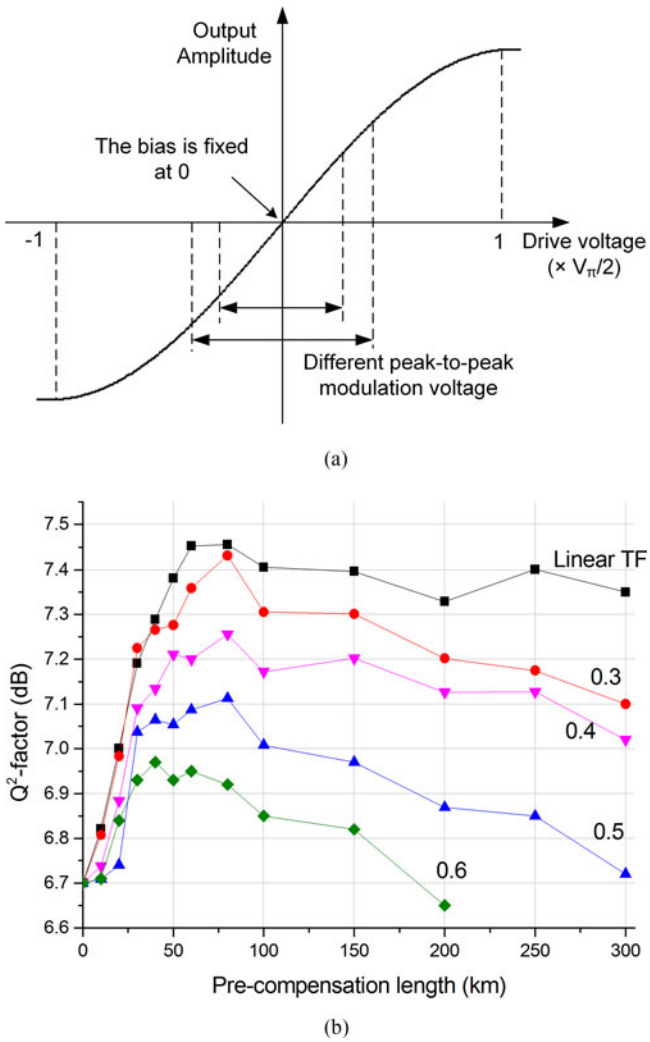

Fig. 5. (a) Nonlinear transform function of modulator, (b) Performance of split-DBP with different signal modulation voltages.

B. Nonlinear Transfer Function of the Modulator

In the practical systems, the nonlinear TF of the modulator is inevitable, which will impact the performance of the transmitter-side DSP algorithms. In the simulations, a typical sinusoidal transform function of the modulator was adopted to evaluate the impact of the nonlinearity of modulator on the split-DBP. For simplicity, the TF of modulator was normalized. The bias was fixed at 0 and the signal was modulated with different modulation voltages to suffer different degrees of nonlinearity. As shown in Fig. 5(a), higher peak-to-peak modulation voltage

would bring more nonlinearity to the signal. With the same incident power of 7 dBm, the signal was modulated with different modulation voltages. The results are shown in Fig. 5(b).

In Fig. 5(b), the horizontal axis denotes the compensation length of transmitter-side DBP (pre-compensation) and the vertical axis the Q^2-factor of the signal after receiver-side DSP. The legends 0.3, 0.4, 0.5 and 0.6 denote the normalized modulation voltages. Among these different modulation voltages, the nonlinearity of the modulator was the most severe with modulation voltage 0.6, and the least severe with modulation voltage 0.3. Linear TF denotes that there was no nonlinearity of the modulator. As we can see, when the TF of the modulator was linear, the best performance appeared when the transmitter-side compensation length was 60 km, and with the transmitter-side compensation length increasing, the Q^2-factor of the signal kept a relative high value. This is because the signal power near the transmitter is much higher than the remainder part of the fiber, the fiber nonlinearity concentrates on the near-transmitter part, and the transmitter-side DBP can avoid the impact of the noise accumulated in the link, as analyzed in Section II.

In contrast, when the TF of modulator was nonlinear, the performance of split-DBP degraded when the nonlinearity increased. Moreover, the performance of split-DBP degraded with the transmitter-side compensation length increasing, because of the errors due to the nonlinear TF accumulated in the fiber transmission. When the modulator nonlinearity was strong enough, the performance of the complete transmitter-side DBP would be worse than the receiver-side DBP. It indicates that the nonlinear TF of modulator will severely degrade the performance of split-DBP, and mitigation of the nonlinearity of the modulator is necessary.

C. Power Profile Mismatch

In bi-directional Raman amplified system, the power profile in DBP should be symmetrical to the power profile in the physical link, as shown in Fig. 1(a). However, in the practical system, the exact signal power distribution in the fiber is hard to measure, and the power profile used in the DBP is calculated by solving the power coupled equations. So there is an issue that the power profile calculated using power coupled equations is not the same as the practical power profile, that is, the power profile used in DBP is not matched with the power profile in physical link. To evaluate the impact of power profile mismatch on the performance of split-DBP, different power profiles were applied in DBP, and the results were compared with the ideal condition.

Fig. 6(a) shows the power profiles used in the split-DBP. Power profile (1) was the same as the power profile in the transmission simulation, and power profile (2), (3) were the power mismatch cases. The forward and backward gains of the three power profiles are shown in Table I. As we can see from Fig. 6(a), power profile (2) had higher power than power profile (1) in the fiber near the transmitter, and in power profile (3), the power in the near-transmitter part was lower than the power profile (1). Fig. 6(b) shows the simulation results of the 3 power profiles. Among the 3 power profiles, the best performance of split-DBP was the case of power profile (2) at the point that the pre-compensation length was 40 km, and the worst performance was the case of power profile (3). In the case of power profile (2), because the power in the near-transmitter part is higher, transmitter-side DBP is over compensation, and the over compensation of fiber nonlinearity will slightly improve the performance of split-DBP when the pre-compensation length is not very long. But with the pre-compensation length increasing, the error due to over compensation accumulates and the performance of split-DBP degrades fast. For the case of power profile (3), the performance curve is similar to but overall worse than the case of power profile (1).

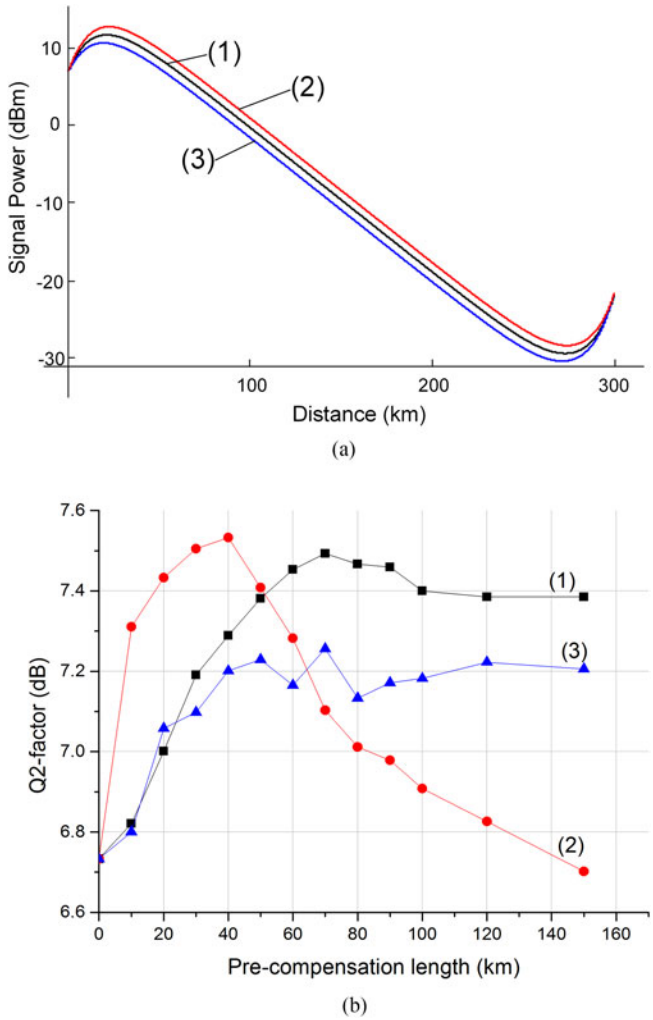

Fig. 6. (a) Power profiles used in DBP, (b) Performance of split-DBP with different power profiles.

TABLE I
THE FORWARD AND BACKWARD GAIN OF THE POWER PROFILES

Power profile	Forward gain (dB)	Backward gain (dB)
(1)	12.4	16.6
(2)	13.6	15.4
(3)	10.6	18.4

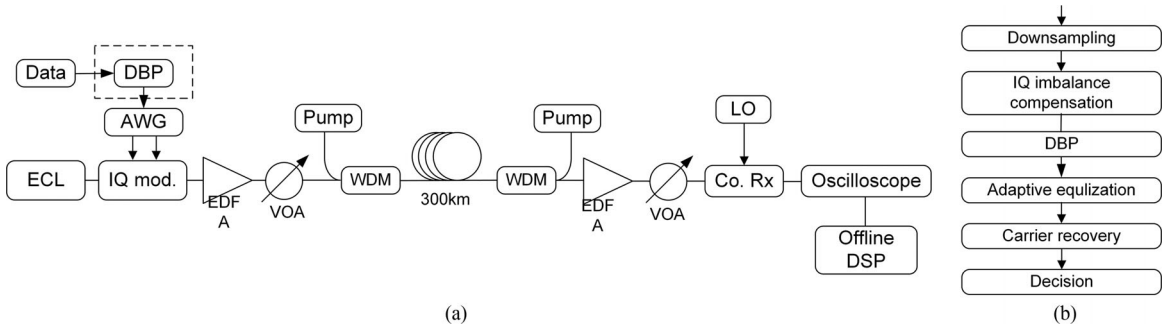

Fig. 7. (a) Experiment setup, ECL: external cavity laser, AWG: arbitrary waveform generator, IQ mod.: IQ modulator, VOA: variable optical attenuator, LO: local oscillator, Co. Rx: coherent receiver; (b) Offline DSP chain.

The simulation results give some guidance on the practical implementation of split-DBP in bi-directional Raman systems. It is obvious that the exact power profile should be used to get the best performance of the split-DBP. In practice, however, the practical power profile in the system is not exactly known. Form the results of Fig. 6(b), it can be seen that when the pre-compensation length is long enough, for example 100 km, the performance of the exact power profile had the best performance, and it helps us to find the optimal power profile in the practical implementation of split-DBP. First, the pre-compensation length should be set to a relatively large value, for example 100 km. Then different power profiles are tested in the split-DBP, and we can get the curve of the relationship between the performance of the split-DBP and power profiles. The power profile with the best performance can be regarded as the exact power profile of the system. After the power profile is found, we can test various pre-compensation lengths to find the optimal pre-compensation length, and finally, the best performance of split-DBP can be obtained.

V. Experiments

Because of the limited experimental conditions, the experiments were only implemented in the case of 10 GBd. The experimental configuration is shown in Fig. 7(a). At the transmitter, an external cavity laser (ECL) of 100 kHz linewidth and 1550.12 nm wavelength was used as the source. The carrier was modulated by an IQ modulator, driven by an arbitrary waveform generator (AWG) with a sample rate of 20 GHz. A pseudo-random binary sequence of $2^{15}-1$ length was generated offline and mapped to 16 QAM digital signal. The signals were generated 2 samples per pulse. In the split-DBP scheme, the signals should be preprocessed with transmitter-side DBP, whereas in the complete receiver-side DBP scheme, they were not preprocessed, and hence the digital signals were converted to analog waveform by AWG and modulated on the carrier. Considering that the nonlinear transfer function of the IQ modulator will impact the performance of transmitter-side DSP algorithm, the electric signal was attenuated with a 9 dB attenuator to remain in the quasi-linear area. Though this method did not fully utilize the modulation range of the modulator, it guaranteed the effectiveness of transmitter-side algorithms. In the experiment, the voltage of the electric signal was adjusted for the best performance of the transmitter-side DBP. After the IQ modulator, the signals were amplified by an EDFA, and then by a variable optical attenuator (VOA) to control the incident power.

The transmission link was a 300 km-long standard single mode fiber. The signals were amplified by a forward and backward distributed Raman amplifier. The pump powers of the forward and backward Raman amplifier were 450 mW and 500 mW, respectively. And, the wavelength of each of the two pump lasers was 1455 nm. After fiber transmission, an EDFA and a VOA were adopted to adjust the signal power into the balanced photodetector (PD). Another ECL of the same parameters as that of the transmitter was used as the local oscillator of coherent reception. After the coherent receiver, the signals were sampled by a digital sampling oscilloscope with a sample rate of 50 GS/s. The sampled digital signals were processed with offline DSP algorithm. Limited to the experimental conditions, the system was performed on single polarization state.

The offline DSP algorithm is illustrated in Fig. 7(b). The digital signals were initially down sampled to two samples/symbols for subsequent processing. Then the Gram-Schmidt orthogonalization procedure (GSOP) was applied to compensate for the IQ imbalance, caused by the imperfections in the modulator and coherent receiver. Subsequently, the DBP algorithm was used to compensate for dispersion and nonlinearity. After DBP, an adaptive equalizer with Constant Modulus Algorithm (CMA) was adapted to compensate for the Inter-symbol interference (ISI), caused by the electric bandwidth limitation of AWG. Lastly, carrier recovery algorithm was applied to compensate for the frequency shift and phase shift, and then for a decision.

For comparison, a simulation with the same parameters as the experiment was carried out. To determine the characteristic of the transceiver noise, in the experiment we measured a back-to-back system, which had the same devices as the transmission experiment but without Raman pumps and fiber. In the back-to-back experiment, the received signal was processed with IQ imbalance compensation, carrier recovery and an adaptive filter with Constant Modulus Algorithm, which were the same as the transmission experiment. After the DSP, we calculated the electric SNR of the signal though the error vector magnitude (EVM):

$$SNR = \frac{1}{|EVM|^2} \tag{4}$$

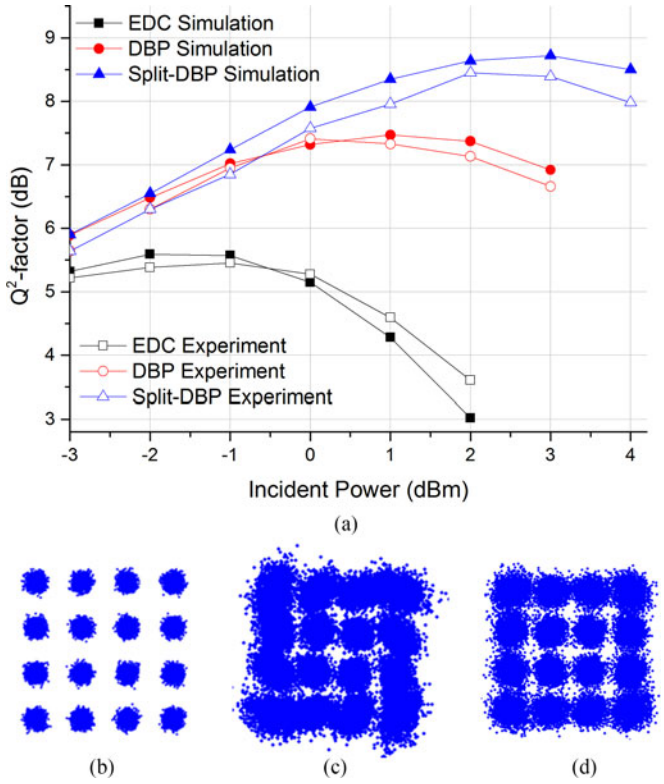

Fig. 8. (a) Q^2-factor vs. incident power in the simulations and experiments with different compensation schemes, and (b), (c), (d) are the constellations of the transmitter-side signal, the signal after receiver-side DBP with incident power 0 dBm, the signal after split-DBP with incident power 2 dBm in the experiment, respectively.

The electric SNR of the back-to-back was 19.1 dB, and the BER measured was 0, with the data length of $2^{15} - 1$. The constellation of the signal is shown in Fig. 8(b), and the noise characteristic was similar to the additive white Gaussian noise (AWGN), which included the transceiver noise and ASE from the two EDFAs.

In the simulation, the transmitter noise and the receiver noise were assumed as AWGN and added at the transmitter and the receiver. In the simulation, we ensured that the back-to-back electrical SNR of the signal was the same as the back-to-back experiment. However, the measured noise of the back-to-back experiment included both the transmitter noise and the receiver noise, and we had no good method to separate the two kinds of noise. The same back-to-back electric SNR only indicates that the sum of the transmitter noise and the receiver noise in the simulation is the same as the experiment, and the ratio of each noise is unknown. To solve this problem, we selected several transmission experimental results as references. In the simulation, we adjusted the ratio of the transmitter noise and the receiver noise to make the simulation results the same as the referenced experimental results.

The simulation and experimental results are shown in Fig. 8(a). Just as in the simulations in Section IV, different DSP schemes, namely EDC, complete receiver-side DBP, and split-DBP were applied. From Fig. 8(a), we can find that the results of simulation and experiment were matched when EDC or receiver-side DBP was applied and the incident power is lower than 0 dBm. And in the case that split-DBP was applied, or when the incident power was higher than 0 dBm, the curves of the experiment were overall a little lower than the curves of the simulation. This is because in the experiment more negative factors would degrade the performance of signal. In the simulation, the Q^2-factors of the signal in complete receiver-side DBP and split-DBP schemes increased by 1.9 dB and 3.2 dB, respectively, compared to the dispersion compensation, and in the experiment, the values were 1.9 dB and 3.1 dB. The curves of experiment were not as smooth as the curves of simulation, and we attribute it to the experimental error.

Fig. 8(c) and (d) correspond to the constellations of the signals at the optimal incident power with complete receiver-side DBP and split-DBP in the experiment, respectively. It can be seen that the constellation of complete receiver-side DBP is distorted, and that the extra NSNI is already severe when the incident power is 2 dBm. When split-DBP was applied, the distorted constellation could be recovered. This implies that the split-DBP scheme can efficiently mitigate the NSNI in the bi-directional Raman amplified system.

VI. Conclusion

In bi-directional Raman amplified unrepeatered systems with receiver-side DBP, extra NSNI is a critical issue, which limits the performance of receiver-side DBP. According to our analysis, by moving the high-power region of the receiver-side DBP to the transmitter-side, the extra NSNI could be mitigated. The performance of split-DBP algorithm in such a system was investigated through simulations and experiments, using a single-channel 300-km bi-directional Raman amplified unrepeatered system. Through simulations, we find that the nonlinear TF of modulator severely impacts the performance of split-DBP, which should be mitigated in practical implementation of split-DBP. And the impact of power profile mismatch was studied, and the results give some guidance on how to find the optimal power profile and pre-compensation length in the practical implementation of split-DBP in bi-directional Raman systems. The transmission simulations were carried out with 16 QAM modulation and the modulation rates were 32 GBd and 10 GBd. The results showed that the split-DBP can deliver 0.8 dB Q^2-factor improvement for the case of 32 GBd and 1.3 dB for the case of 10 GBd, compared to the traditional DBP. The experimental results indicate that the split-DBP improves the performance of signal by 3.1 dB, compared to the EDC scheme, and by 1.2 dB compared to the complete receiver-side DBP. The simulation and experimental results prove that the split-DBP scheme can efficiently mitigate the NSNI in the system.

Acknowledgment

The authors would like to thank Dr. Shaohua Yu and Dr. Qi Yang for their help on the experiments.

REFERENCES

[1] A. Mohamed, M. AliKarar, and T. andolosi, "DSP-based dispersion compensation: Survey and simulation," in *Proc. ICCCCEE*, Khartoum, Sudan, 2017, pp. 1–7.

[2] A. T. Erdogan, A. Demir, and T. M. Oktem, "Automatic PMD compensation by unsupervised polarization diversity combining coherent receivers," *J. Lightw. Technol.*, vol. 26, no. 13, pp. 1823–1834, Jul. 2008.

[3] R. Essiambre, G. Kramer, P. J. Winzer, G. J. Foschini, and B. Goebel, "Capacity limits of optical fiber networks," *J. Lightw. Technol.*, vol. 28, no. 4, pp. 662–701, Feb. 2010.

[4] E. Ip and J. M. Kahn, "Compensation of dispersion and nonlinear impairments using digital backpropagation," *J. Lightw. Technol.*, vol. 26, no. 20, pp. 3416–3425, Oct. 2008.

[5] E. Ip, "Nonlinear compensation using backpropagation for polarization-multiplexed transmission," *J. Lightw. Technol.*, vol. 28, no. 6, pp. 939–951, Mar. 2010.

[6] R. Maher *et al.*, "Spectrally shaped DP-16QAM super-channel transmission with multi-channel digital back-propagation," *Sci. Rep.*, vol. 5, Feb. 2015, Art. no. 8214.

[7] A. Napoli *et al.*, "Reduced complexity digital back-propagation methods for optical communication systems," *J. Lightw. Technol.*, vol. 32, no. 7, pp. 1351–1362, Apr. 2014.

[8] X. Liang and Shiva Kumar, "Multi-stage perturbation theory for compensating intra-channel nonlinear impairments in fiber-optic links," *Opt. Exp.*, vol. 22, no. 24, pp. 29733–29745, Dec. 2014.

[9] H. Yao *et al.*, "A modified adaptive DBP for DP 16-QAM coherent optical system," *IEEE Photon. J.*, vol. 28, no. 22, pp. 2511–2514, Nov. 2016.

[10] L. Galdino *et al.*, "On the limits of digital back-propagation in the presence of transceiver noise," *Opt. Exp.*, vol. 25, no. 4, pp. 4564–4578, Jan. 2017.

[11] N. V. Irukulapati, H. Wymeersch, P. Johannisson, and E. Agrell, "Stochastic digital backpropagation," *IEEE Trans. Commun.*, vol. 62, no. 11, pp. 3956–3968, Nov. 2014.

[12] D. Lavery, D. Ives, G. Liga, A. Alvarado, S. Savory, and P. Bayvel, "The benefit of split nonlinearity compensation for single channel optical fiber communications," *IEEE Photon. Technol. Lett.*, vol. 28, no. 17, pp. 1803–1806, Sep. 2016.

[13] D. Lavery, R. Maher, G. Liga, D. Semrau, L. Galdino, and P. Bayvel, "On the bandwidth dependent performance of split transmitter-receiver optical fiber nonlinearity compensation," *Opt. Exp.*, vol. 25, no. 4, pp. 4554–4563, 2017.

[14] Z. Xiao *et al.*, "Low complexity split digital backpropagation for digital subcarrier-multiplexing optical transmissions," *Opt. Exp.*, vol. 25, no. 22, pp. 27824–27833, 2017.

[15] Jake Bromage, "Raman amplification for fiber communications systems," *J. Lightw. Technol.*, vol. 22, no. 1, pp. 79–93, Jan. 2014.

[16] W. S. Pelouch, "Raman amplification: An enabling technology for long-haul coherent transmission systems," *J. Lightw. Technol.*, vol. 34, no. 1, pp. 6–19, Jan. 2016.

[17] L. Galdino *et al.*, "Amplification schemes and multi-channel DBP for unrepeatered transmission," *J. Lightw. Technol.*, vol. 34, no. 9, pp. 2221–2227, May 2016.

[18] G. Saavedra, D. Semrau, L. Galdino, R. I. Killey, and P. Bayvel, "Digital back-propagation for nonlinearity mitigation in distributed Raman amplified links," *Opt. Exp.*, vol. 25, no. 5, pp. 5431–5439, 2017.

[19] P. Gysel and R. K. Staubli, "Statistical properties of Rayleigh backscattering in single-mode fibers," *J. Lightw. Technol.*, vol. 8, no. 4, pp. 561–567, Apr. 1990.

[20] G. P. Agrawal, *Nonlinear Fiber Optics*. New York, NY, USA: Academic, 2007.

[21] V. Kalavally, I. D. Rukhlenko, M. Premaratne, and T. Win, "Analytical study of RIN transfer in pulse-pumped raman amplifiers," *J. Lightw. Technol.*, vol. 27, no. 20, pp. 4536–4543, Oct. 2009.

Qiang Zheng is currently working toward the Ph.D. degree in optical engineering at Huazhong University of Science and Technology, Wuhan, China.

Liyan Huang has worked on the Raman amplified systems for several years. She is currently an Engineer with Accelink Technologies Co., Ltd., Wuhan, China.

Wei Li received the Ph.D degree from Huazhong University of Science and Technology, Wuhan, China. She is currently a Professor with Wuhan National Lab for Optoelectronics, Huazhong University of Science and Technology. Her research focuses on the optical communication technology and devices.

Qiguang Feng is currently working toward the Ph.D. degree in optical engineering at Huazhong University of Science and Technology, Wuhan, China.

Chengpeng Fu has worked on the Raman amplifier for several years. He is currently an Engineer with Accelink Technologies Co., Ltd., Wuhan, China.

Jiekui Yu has worked on the optical communication system for several years. He is currently an Engineer with Accelink Technologies Co., Ltd., Wuhan, China.